

Sub-Micron Diffractive Optical Elements Facilitated by Intrinsic Deswelling of Auxetic Liquid Crystal Elastomers

Thomas Moorhouse and Thomas Raistrick*

Diffractive optical elements (DOEs) enable precise control over the direction and filtering of light, making them common components in spectrometers, waveguides, and sensors. There is great interest in tunable and sub-micron diffractive optical elements in flexible photonics and for responsive structural colors. Here this study presents sub-micron tunable diffraction gratings produced by patterning a liquid crystal elastomer (LCE). The intrinsic anisotropic deswelling of the liquid crystal elastomer enables sub-micron (707 nm) pitch structures to be produced from a micron-scale (1040 nm) surface relief grating. Using atomic force microscopy (AFM) and diffraction measurements, a thermal pitch tunability is demonstrated of +212 nm (+31%) or −322 nm (−33%) over a temperature range of 215 °C depending on grating orientation. A mechanical pitch tunability is demonstrated of +1110 nm by applying strains of up to 157% to the liquid crystal elastomer. The height of the diffraction grating is preserved over strain due to the negative Poisson-ratio, or “auxetic”, behavior exhibited by this chosen family of the liquid crystal elastomers. This report opens the possibility of using LCEs to facilitate flexible sub-micron diffractive optical elements, with a high degree of tunability for sensing and structural color applications.

production,^[10] and biomedical technology,^[11] similarly requires the production of structures with sub-micron periodicity. Here we present an approach which uses the intrinsic deswelling of liquid crystal elastomers (LCEs) to produce sub-micron DOEs with a high degree of tunability and stimuli responsiveness.

Soft lithography offers a lower cost and more accessible means of surface patterning relative to traditional techniques such as photo- and electron beam- lithography, which rely on expensive systems and complex multistep processes.^[12–14] Miniaturization of surface features with shape-memory polymers provides a feasible approach to sub-micron scale patterning via soft lithography.^[15,16] Subtractive patterning of shape-memory polymers with dry-etch processes introduces an inherent surface roughness that results in a loss of fidelity in a little as one miniaturization cycle.^[15] Achieving high-fidelity sub-micron embedded relief structures using this technique is therefore limited without

1. Introduction

The recent growing interest in elastomeric optical elements, over their solid counterparts, has been driven by an increased demand for device tunability and biocompatibility, and the continued development of flexible electronics and photonics.^[1–5] Many optical devices rely on the production of soft diffractive optical elements (DOEs) with sub-micrometer features, such as soft grating couplers^[6,7] and grating-enhanced solar cells.^[8] The phenomenon of responsive “structural color”, which has far-reaching implications in display devices,^[9] chemical-free textile

additional steps in the process. Solvent-assisted nanoscale embossing instead uses additive patterning of shape-memory polymers and solvent swelling,^[16] providing an alternative miniaturization framework for variable nanostructured surfaces.

The use of LCEs, presented herein, provides another layer of tunability to existing miniaturization frameworks due to their inherent anisotropic deswelling properties^[17,18] and stimuli responsiveness (thermal, mechanical, photo and chemical). LCEs are lightly cross-linked polymeric materials containing, typically rod-like, mesogenic units within their network (**Figure 1a**). The coupling between liquid crystal order and the macroscopic shape of an LCE leads to stimuli-induced shape actuation.^[19] Further, the formation of the LCE network in the presence of a solvent and its subsequent removal results in a controllable anisotropic deswelling of the network.

Intrinsic anisotropic deswelling has been leveraged to produce chiral nematic LCEs with structural color by physically restraining the sample whilst deswelling^[18]; the simplicity of this technique allows for easy scalability to industry relevant sizes. In this report, we leverage the facile anisotropic deswelling of LCEs to produce sub-micron scale DOEs using alignment techniques common and relevant to the liquid crystal display industry. As the alignment of the LCE can be tailored with respect to the grating, the use of nematic LCEs and a nematic solvent allows for responsiveness to be optimized for the desired

T. Moorhouse, T. Raistrick
School of Physics and Astronomy
University of Leeds
Leeds LS2 9JT, UK
E-mail: T.J.Raistrick@leeds.ac.uk

The ORCID identification number(s) for the author(s) of this article can be found under <https://doi.org/10.1002/adom.202400866>

© 2024 The Author(s). Advanced Optical Materials published by Wiley-VCH GmbH. This is an open access article under the terms of the [Creative Commons Attribution](#) License, which permits use, distribution and reproduction in any medium, provided the original work is properly cited.

DOI: 10.1002/adom.202400866

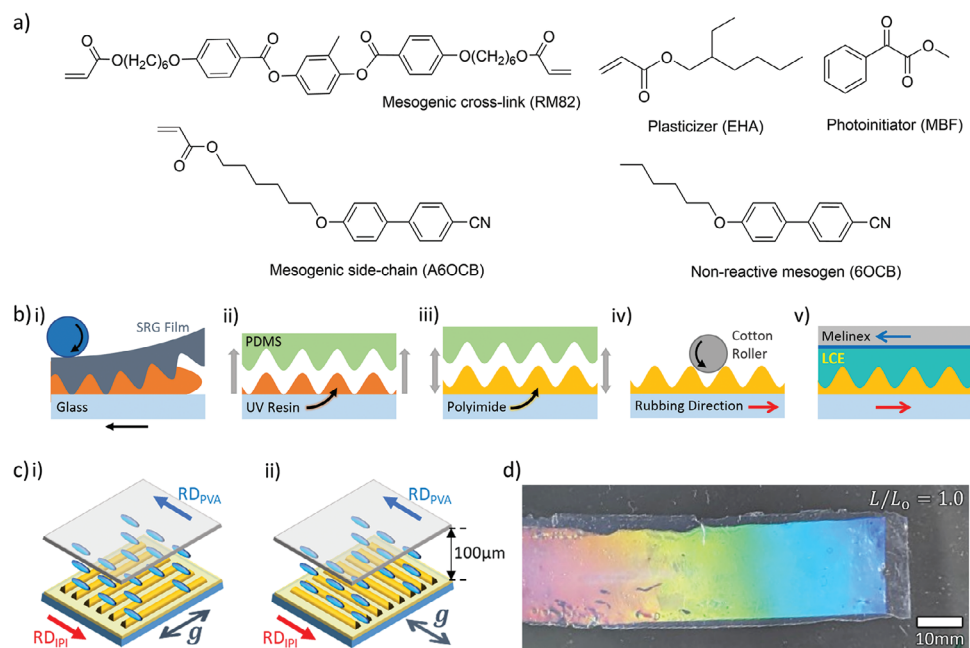


Figure 1. Fabrication method for producing nematic LCEs with micron and sub-micron features, labelled as μ LCEs. a) Chemical structures of constituent chemicals used to synthesize nematic LCEs. The non-reactive mesogen, 6OCB, is removed after polymerization by washing the LCE in solvent, resulting in anisotropic deswelling. b-i) A linear SRG film is embossed in to UV curable resin on a glass backing. ii) A polydimethylsiloxane (PDMS) working stamp is made via replica molding. iii) A spin coated layer of polyimide is imprinted with a PDMS working stamp. iv) The imprinted polyimide (IPI) surface is mechanically rubbed using a cotton roller. v) A LCE mixture fills the 100 μ m thick cavity, between a rubbed IPI surface and a rubbed, PVA coated Melinex® film. The polymerized LCE is demolded, washed and dried, forming a μ LCE film. c) Device construction used in μ LCE fabrication, indicating IPI and PVA rubbing directions (RD_{IPI} , RD_{PVA}) and IPI SRG groove orientation (g) for i) director perpendicular to g and ii) director parallel to g . d) Image of nematic μ LCE film.

response, i.e., pitch reduction upon increasing temperature and vice-versa.

Due to their stimuli-responsive nature, LCEs are ideal candidates for sensor applications enabled by their highly-tunable optical and mechanical properties.^[5,19–22] LCEs have previously been used to form stimuli-responsive diffraction gratings,^[23,24] however these previous reports did not explore the production of gratings on the sub-micron length scale. In these earlier reports, the diffractive effect is induced via refractive index modulation across a sample by exploiting cis-trans isomerization of azo-benzene mesogenic units.^[23,24] These refractive index modulated diffractive LCEs show high sensitivity to changes in temperatures, but given the micron-scale grating dimensions, the achieved diffraction angles were small, limiting the applicability of these materials. Similarly, Zhang et al. recently reported a soft lithographic approach to produce periodic topographical features on an LCE by imprinting a partially cross-linked LCE gel with a 6.7 micron pitch surface relief grating (SRG).^[25] A second cross-linking step was performed under strain to produce a macroscopically aligned, and therefore stimuli shape-responsive, LCE with a 11.7 micron pitch grating. Upon heating to 84 °C, the imprinted pitch contracted to 7.8 micron (–33%). Whilst Zhang et al. demonstrates the stimuli-responsiveness of imprinted LCE gratings, a pitch smaller than the initial SRG was not reported and miniaturization of surface features was not achieved.

In this work, we report a new method for realizing LCE DOEs with sub-micron scale features, via solvent mediated miniaturiza-

tion. Molds are constructed with an imprinted polyimide (IPI) SRG alignment layer (1040 nm pitch). The use of a polyimide substrate allows for conventional rubbed alignment to be applied to the grating structures, overriding their inherent topographic influence on the director orientation.^[26] This rubbed grating technique, used previously for characterizing polyimide anchoring strengths in low molar mass liquid crystal devices, is applied to LCE device fabrication for the first time, allowing the swollen LCEs to be formed with an arbitrary director alignment relative to the grating orientation (outlined in Figure 1b,c).

Our approach has been to use a class of all-acrylate LCEs which are synthesized in the presence of non-reactive liquid crystalline components, producing an inherently swollen network upon polymerization^[27,28] (chemical components shown in Figure 1a). Removal of the non-reactive liquid crystalline component causes a controllable anisotropic deswelling of the network enabling miniaturization of surface features. The LCEs used here are unique as they deform via a “mechanical Fréedericksz transition” and they display a negative Poisson ratio (or “auxetic”) response under mechanical deformation.^[28–30] Using atomic force microscopy (AFM), we observed an auxetic response when measuring the height of the grating on the LCE, i.e., the grating features increase in height as the films are subjected to tensile strains. Thus, these LCEs may overcome the diffraction efficiency losses associated with surface feature height reduction under strain, which is a fundamental issue with elastomeric DOEs.^[12] Other more conventional LCEs deform via a different mechanism, known as semi-soft elasticity and is characterized by the

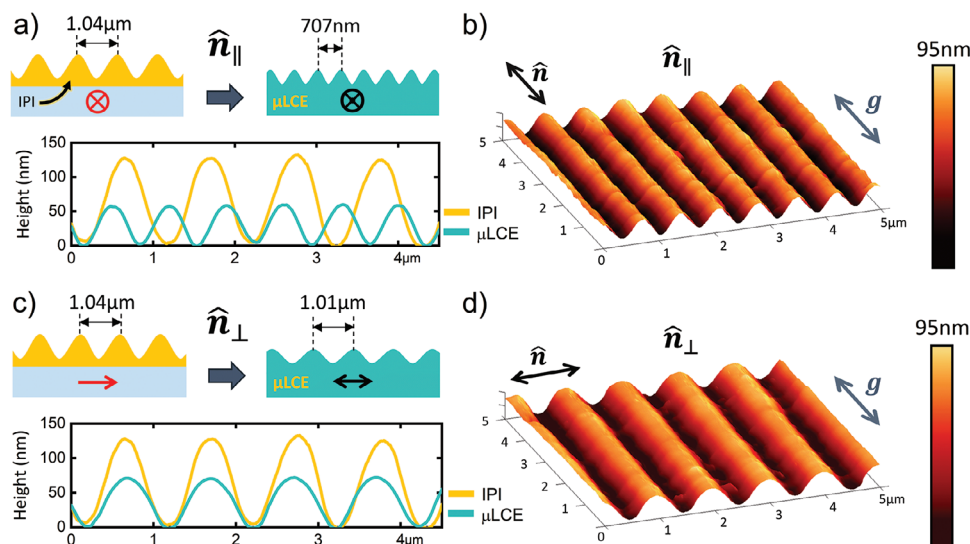


Figure 2. AFM surface profilometry of nematic μ LCE films at 20 °C. The plots in (a,c) include AFM surface profiles of the IPI SRG molds (yellow) used during fabrication (pitch = 1040 ± 5 nm, height = 130 ± 5 nm), highlighting the reduced dimensions of the μ LCEs (cyan). a,b) \hat{n}_{\parallel} μ LCE fabricated on an IPI surface with the nematic director (\hat{n}) aligned parallel to the SRG grooves (g) (pitch = 707 ± 10 nm, height = 53 ± 3 nm). (c, d) \hat{n}_{\perp} μ LCE fabricated on an IPI surface with \hat{n} aligned perpendicular to g (pitch = 1010 ± 5 nm, height = 68 ± 3 nm).

appearance of “stripe domains”, which involves counter-rotating domains that strongly scatter light^[31,32] and thus limit their applications as stretchable DOEs. By comparison, these LCEs, which deform via the so called mechanical Fréedericksz transition, remain optically clear under strain and with affine deformations.^[27] Here, we demonstrate that the imprinted LCEs have a pitch tunability of 1110 nm over a strain range 157% making them ideal candidates for mechanical beam steering applications.

In addition to their response under strain, the all-acrylate LCEs display a highly super-critical response to temperature, displaying near-linear changes in birefringence upon heating when compared to the highly non-linear response of conventional semi-soft elastic LCEs.^[27,33] Here, we demonstrate a temperature-responsiveness of +211 or –322 nm (depending on director orientation with respect to grating grooves) of the LCEs over a temperature range of 215 °C. This report is therefore the first demonstration of sub-micron DOEs produced using LCEs with a high degree of chemical, thermal, and mechanical tunability.

2. Results and Discussion

2.1. LCE DOEs with Sub-Micron Features via Anisotropic Deswelling

The LCEs patterned with micro-scale SRGs, labelled as μ LCEs from here onward, are produced as outlined in the introduction and Figure 1. The use of an imprinted polyimide (IPI) alignment layer allows for the nematic director orientation (\hat{n}) to be aligned at an arbitrary angle with respect to the grating. Here, the effect of director orientation on the topographical features of the μ LCE is demonstrated by synthesizing two LCEs with \hat{n} either parallel (\hat{n}_{\parallel}) or perpendicular (\hat{n}_{\perp}) to the grooves of the IPI SRG (g). Figure 2 shows the topographical features of these LCEs measured with AFM. The anisotropic nature of the deswelling causes

contrasting reductions in pitch for the \hat{n}_{\parallel} or \hat{n}_{\perp} cases. In the \hat{n}_{\parallel} case the pitch is reduced by 32% to 707 nm. This 333 nm pitch reduction, investigated in detail in the following section, demonstrates the ability for sub-micron surface features to be produced from micron-scale SRGs, through the intrinsic anisotropic deswelling of the LCEs (Figure 2a,b). In contrast, minimal pitch reduction is observed in the \hat{n}_{\perp} case which contracts by only 3% (Figure 2c,d). This demonstrates the simplest facet of μ LCE tunability, which is controlling the pitch of the surface features using the rubbing-defined orientation of \hat{n} relative to g , which can vary the resulting pitch, by up to 30%. Rubbing at intermediate angles between parallel and perpendicular to g , may offer incremental control over the deswelling, if calibrated and proven robust. In the vertical (height) dimension, a 59% and 48% reduction in grating height (h) is observed in \hat{n}_{\parallel} and \hat{n}_{\perp} cases respectively. Both varieties result in surface profiles bearing a close resemblance to that of the IPI molds used during fabrication, but with an altered grating pitch and height.

2.2. Composition-Driven Grating Tunability

Alongside director orientation, the concentration of the non-reactive mesogen, 6OCB, provides further dimensional tunability by varying the amount of deswelling that occurs upon its removal post-polymerization. Four μ LCE compositions (chemical compositions outlined in the experimental section) are produced with varying concentrations of 6OCB content and used to fabricate μ LCEs in the \hat{n}_{\parallel} configuration (Figure 1c–ii). The LCE marked with an asterisk (*) is the composition used in Section 2.1 and the remainder of this report. Figure 3 shows the pitch and height (measured by AFM) of the μ LCEs with varying 6OCB concentrations.

AFM profile scans of the μ LCEs with varying 6OCB concentration are shown in Figure 3a, where both the pitch and height

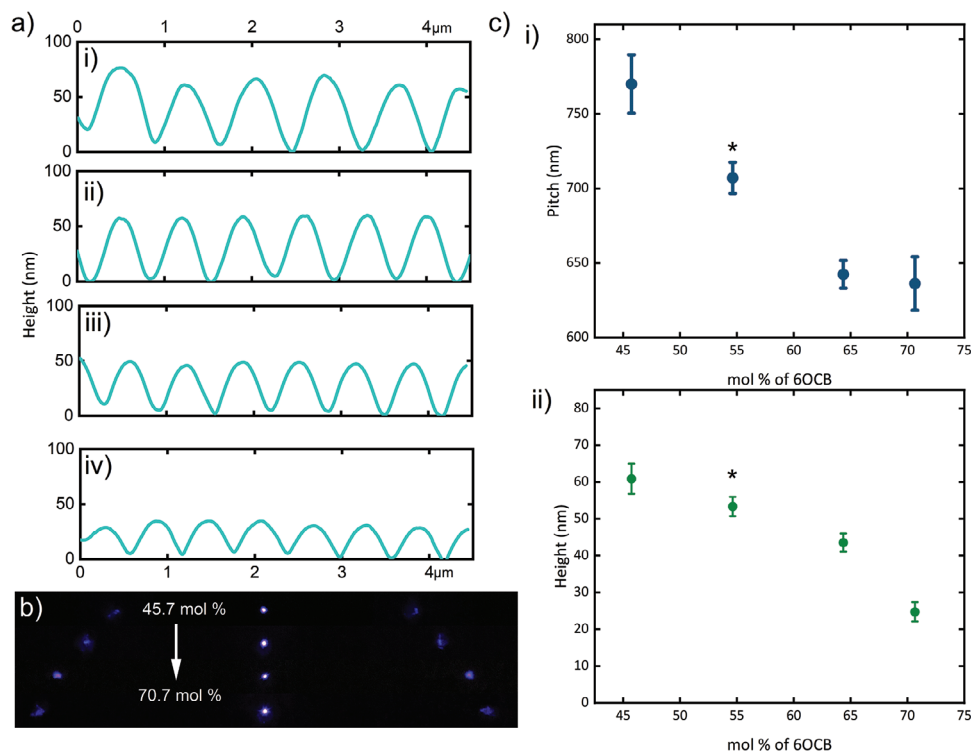


Figure 3. Compositional dependence of \hat{n}_{\parallel} μ LCEs on the concentration of 6OCB present in the LCE precursor mixture. a) AFM surface profilometry of the \hat{n}_{\parallel} μ LCEs with i) 45.7 mol.%, ii) 54.6 mol.%, iii) 64.4 mol.% and iv) 70.7 mol.% of 6OCB in the precursor mixture. b) Compositional dependence of i) pitch and ii) height on concentration of 6OCB in precursor mixture as measured by AFM. Chemical composition used in the previous and subsequent sections of this report is marked with an asterisk. c) Diffraction patterns of the \hat{n}_{\parallel} μ LCEs upon increasing mol concentration of 6OCB.

of the resulting μ LCE gratings display an inverse non-linear relationship with 6OCB concentration (Figure 3b), showing that compositional changes impact both lateral and vertical feature dimensions simultaneously. For example, the 64.4 mol% 6OCB sample has a 38% and 52% decrease in pitch and height respectively, whereas the 45.7% 6OCB sample displays a 32% and 65% decrease in pitch and height respectively, when compared to the IPI SRG mold. The diffraction patterns of the μ LCEs for the various compositions is shown in Figure 3c.

Previously, anisotropic deswelling has been used to form chiral nematic and smectic LCEs, where a partially cross-linked isotropic gel was synthesized in toluene and mechanical fields are then applied.^[17,18,34] During evaporation of the toluene, alignment is achieved by deswelling combined with the final cross-linking step. Here, instead we use a non-polymerizable nematic component, 6OCB, in the LCE precursor mixture. The presence of 6OCB allows for the monomer mixture to be a nematic liquid at room temperature, which means surface alignment can be achieved before polymerization. The aligned LCE precursor produces monodomain nematic LCE films upon UV irradiation. As such, there is a requirement for the LCE precursor mixture to be sufficiently deep within the nematic phase, to allow for high quality monodomain alignment, and sufficiently far away from the point at which crystallization/solid formation occurs. These two requirements set the range for the amount of 6OCB that can be included in the LCE precursor mixture and the extent of anisotropic deswelling that can be currently achieved.

The nematic-to-isotropic transition temperature, T_{ni} , of the precursor mixtures were determined via differential scanning calorimetry (DSC) on cooling at a rate of $10 \text{ }^{\circ}\text{C min}^{-1}$. The 45.7 mol% 6OCB precursor mixture has a T_{ni} of $30.4 \text{ }^{\circ}\text{C}$ whilst the 70.7 mol.% 6OCB precursor mixture has a T_{ni} of $49.5 \text{ }^{\circ}\text{C}$ (Figure S1, Supporting Information). UV polymerization is performed at room temperature ($25 \text{ }^{\circ}\text{C}$) which is $5.4 \text{ }^{\circ}\text{C}$ and $24.5 \text{ }^{\circ}\text{C}$ below T_{ni} for the 45.7 mol% and 70.7 mol% 6OCB precursor mixture respectively. For the 45.7 mol% 6OCB precursor mixture, the polymerization temperature may not be sufficiently below T_{ni} to allow for the high quality monodomain alignment required for surface features with uniform pitch and amplitude (Figure 3a,b) to be achieved. During μ LCE production, the LCE precursor mixture is left to surface align for 20 min. The 70.7 mol% 6OCB sample was also found to be spatially inhomogeneous (Figure 3b plots the average of the measured pitch values, 664 ± 15 and $597 \pm 13 \text{ nm}$, for different areas of the 70.7 mol% 6OCB sample). Whilst the 70.7 mol% 6OCB precursor mixture is polymerized deep within the nematic phase, the precursor mixture is prone to phase separation and partial crystallization as evidenced by a cold-crystallization and melting peak on DSC traces (Figure S1, Supporting Information). The spatially inhomogeneous pitch observed in the sample with 70.7 mol% 6OCB (Figure 3a,b) is therefore related to partial crystallization during polymerization. Thus, the nematic-to-isotropic transition temperature and the stability of the precursor mixture limits the range of pitches which are practically attainable via anisotropic deswelling.

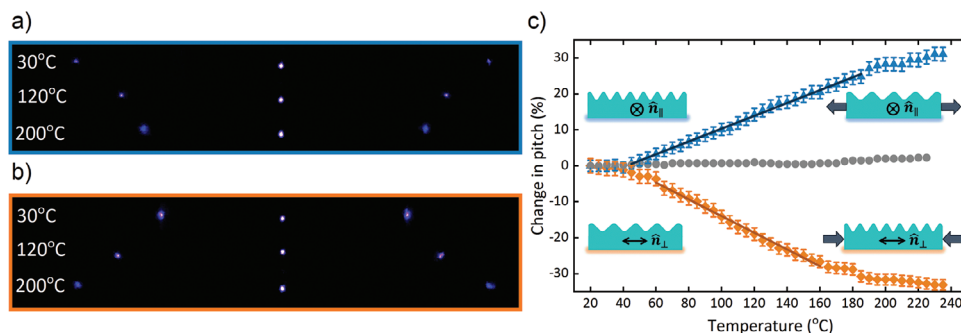


Figure 4. Thermal response of the \hat{n}_{\parallel} and \hat{n}_{\perp} μ LCE via optical diffraction measurements. a,b) Diffraction patterns showing the opposing thermal responses of \hat{n}_{\parallel} and \hat{n}_{\perp} μ LCEs, where \hat{n}_{\parallel} exhibits pitch expansion (a) and \hat{n}_{\perp} exhibits pitch contraction (b) respectively upon heating. c) The relative thermal change in grating pitch of \hat{n}_{\parallel} (blue triangles) and \hat{n}_{\perp} (orange diamonds) nematic μ LCE films determined from diffraction measurements. The gray circles in (c) are the relative thermal changes in pitch for an isotropic sample of the same composition.

2.3. Thermal Response of μ LCEs

The thermal response of the μ LCEs is investigated by diffraction angle measurements over a temperature range of 20–235 °C using a 404 nm laser with a 1.5 mm spot size. The \hat{n}_{\parallel} μ LCE exhibits pitch expansion upon heating (Figure 4a), indicated by a decrease in diffraction angle ($\Delta\theta < 0$) of up to 10° over the full temperature range, corresponding to a 212 nm increase (+31%) in pitch relative to the sample at 20 °C. Conversely, the \hat{n}_{\perp} μ LCE exhibits pitch contraction upon heating (Figure 4b), indicated by an increase in diffraction angle ($\Delta\theta > 0$) of up to 14° over the full temperature range. This corresponds to a 322 nm reduction (−33%) in pitch relative to the sample at 20 °C. The \hat{n}_{\parallel} and \hat{n}_{\perp} μ LCEs both exhibit broad, near-linear regimes in their thermal response due to the supercritical nature of this class of LCEs.^[27] Figure 4c shows linear fits over selected temperature ranges for the μ LCEs where the response is most linear; the slopes of which indicate thermal sensitivity. The pitch of the \hat{n}_{\parallel} sample has a thermal sensitivity of $1.2 \pm 0.1 \text{ nm } ^\circ\text{C}^{-1}$ (taken from a linear fit over 40–185 °C) whereas the pitch of the \hat{n}_{\perp} sample exhibits a higher thermal sensitivity of $-2.2 \pm 0.1 \text{ nm } ^\circ\text{C}^{-1}$ (taken from a linear fit over 60–160 °C). Figure 4c also shows data for an isotropic μ LCE, which has an identical chemical composition to its nematic counterpart, but is instead polymerized in the isotropic phase, as described previously.^[20] The isotropic μ LCE does not shape actuate and has a thermal sensitivity of $0.21 \text{ nm } ^\circ\text{C}^{-1}$, which can be attributed to the general thermal expansion of isotropic materials. This demonstrates the importance of, and uniqueness offered by, anisotropy in the thermal actuation response of the nematic μ LCE diffraction gratings.

2.4. Strain Response of μ LCEs

Application of tensile strain changes the macroscopic dimensions of the μ LCE and thus the dimensions of the grating structure embedded in the surface. Mechanical tests are performed on the \hat{n}_{\parallel} μ LCE with strains applied perpendicular to \hat{n} and g . A linear increase in pitch of up to 1110 nm (167% as measured by diffraction) is observed as the LCE is stretched by a factor of 156%. We also characterized the surface topography of the strained μ LCE via AFM, imaged at multiple strain levels over the range tested

during diffraction measurements. Figure 5a shows good agreement between the pitch values obtained via diffraction and AFM.

In contrast to diffraction measurements, AFM enables the grating depth/height (h) to be directly measured. AFM results therefore reveal the consequences of the selected LCE's auxetic nature on the μ LCE grating, in the form of nanoscale growth in feature height at large strains. At a moderate 41% strain, h is reduced by 10% relative to the initial unstrained height (h_0). This height reduction in the grating is consistent with the initially positive Poisson's ratio (i.e., non-auxetic) tensile response of this LCE.^[28,30] However, upon further straining to 82% and 146% strain, the feature height increases and exceeds its initial, unstrained height by 10% and 26% respectively. This behavior is attributed to the onset of the auxetic response (Figure 5b). We add that the measured auxetic growth of 13 nm between 0% and 146% strain, is significantly larger than the $\pm 3 \text{ nm}$ error in the average height of unstrained μ LCE, thus the measured effect is not due to spatial variation in feature height but a real phenomenon and manifestation of the bulk material's auxetic response. Curiously, the auxetic response in grating height, measured via AFM, exceeds the height of the original grating. This is a distinctly different response to that seen in the bulk dimensions of auxetic LCEs, where the samples never exceed their original thickness.^[28–30] Therefore this suggests that the auxetic response of the LCE is enhanced at the surface, on the nanometer scale, when compared to the bulk response. The AFM surface profiles plotted in Figure 5c emphasize this unique topographic response, showing the linear increase in pitch and non-linear variation in height as the fractional length is increased.

2.5. Diffraction Efficiency of μ LCEs

The 1st order diffraction efficiency of the μ LCEs is investigated under heating and the application of strain, as shown in Figure 6. The grey dashed line on each subfigure is the theoretically predicted efficiency for a sinusoidal grating profile, described by Meshalkin et al.^[35] and provided in Equations (1) and (2).

$$\Delta\phi = \frac{2\pi}{\lambda} (h(n-1)) \quad (1)$$

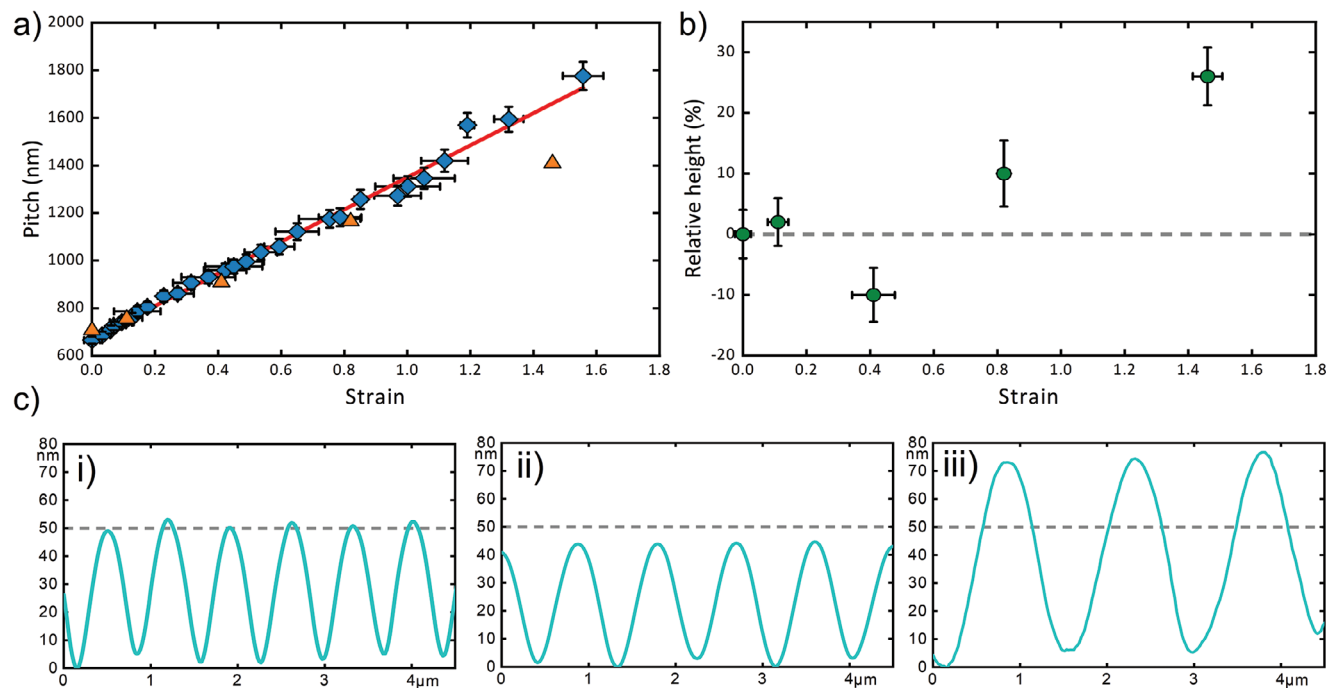


Figure 5. Tensile strain testing on \hat{n}_{\parallel} nematic μ LCE. a) Relationship between grating pitch (d) and strain. Pitch measurements are taken using optical diffraction patterns (diamonds) and AFM (triangles). b) Relative height (h) of the μ LCE surface relief grating as a function of strain, measured via AFM. Dashed horizontal lines denote the static height (h_0). c) Cross-sectional line profiles from AFM scans of the μ LCE i) at rest, ii) at 41% strain and iii) at 146% strain.

$$\eta_1 = \frac{4}{\pi^2} \sin^2\left(\frac{\pi}{2}\right) \sin^2(\Delta\phi) \quad (2)$$

where $\Delta\phi$ is the phase difference, h is the grating depth and n is the refractive index of the material. Here, circularly polarized light is used and we use the average refractive index, n , which is taken to be a single value 1.57^[36] in the theoretical prediction. The agreement between theoretical predictions and measured values validates this approach. The measured diffraction efficiency is comparable to the previously reported diffraction efficiency of refractive index modulated diffraction gratings on LCEs (0.7% at room temperature, 1.2% peak efficiency).^[23]

The diffraction efficiency upon heating of the n_{\parallel} and n_{\perp} μ LCE is shown in Figure 6a,b respectively where either an increase (n_{\parallel}) or decrease (n_{\perp}) in diffraction efficiency is observed. The changes in diffraction efficiency cannot be solely related to changes in refractive index upon heating as in both cases the refractive index decreases.^[36] The result may be understood in part due to the changes in pitch observed in Figure 4. Very low modulation gratings have a peak efficiency at $\lambda_p = 3.4 \times ad$ where $a = h/d$ is the modulation, h is the grating depth and d is the groove spacing.^[37] Substituting values into this, λ_p is 180 nm and 231 nm for the n_{\parallel} and n_{\perp} μ LCE respectively at room temperature. The diffraction efficiency measurements are performed using a 404 nm laser. Upon heating the pitch increases for n_{\parallel} , therefore, λ_p shifts closer

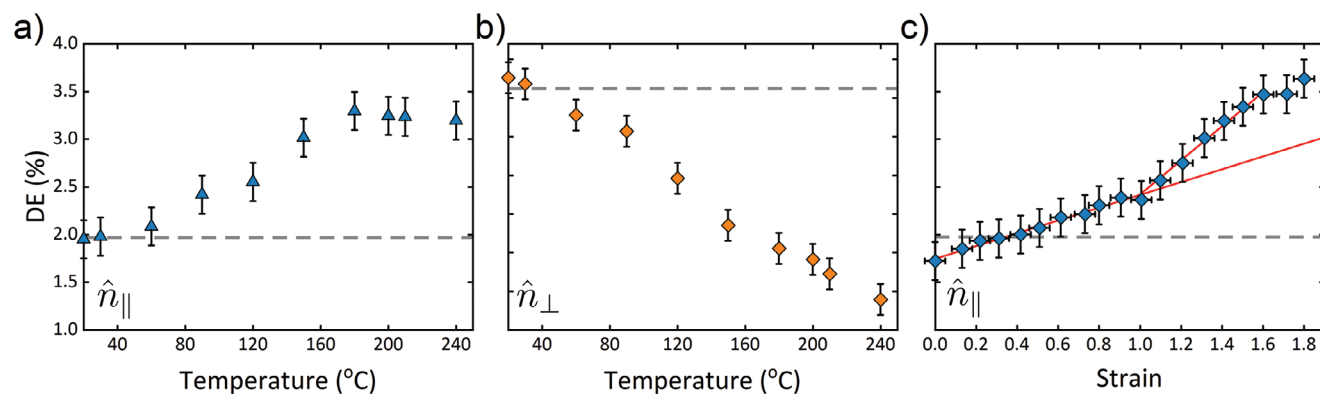


Figure 6. 1st order diffraction efficiency (DE) of the μ LCEs under various conditions. a,b) n_{\parallel} and n_{\perp} μ LCE upon heating, c) n_{\parallel} μ LCE under strain. The grey dotted line is the theoretical predicted efficiency for the given grating depth and laser wavelength.

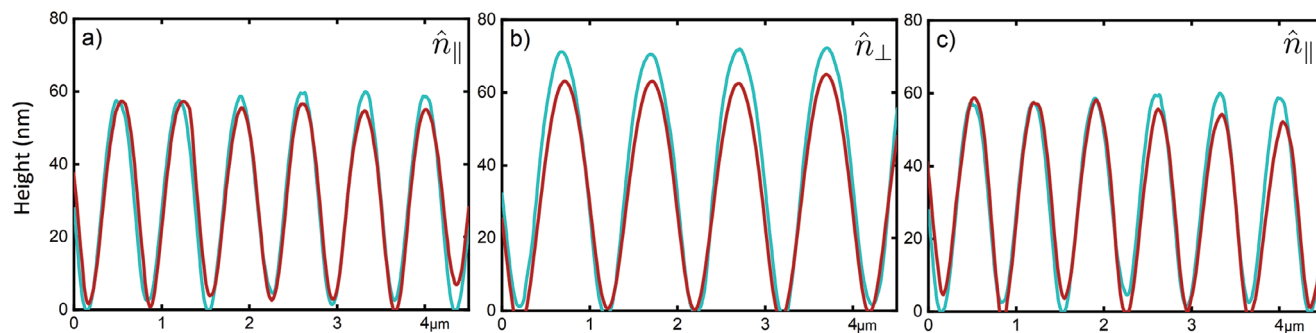


Figure 7. AFM surface profilometry of nematic μ LCE films. a) $n_{||}$ μ LCE pre- (cyan) and post- (red) heating to 240 °C. b) n_{\perp} μ LCE pre- (cyan) and post- (red) heating to 240 °C. c) $n_{||}$ μ LCE pre- (cyan) and post- (red) straining to 156%.

toward 404 nm and an increase in efficiency is observed. Conversely, the pitch decreases for n_{\perp} , and λ_p shifts away from 404 nm and a decrease in efficiency is observed. It is noteworthy that this is an optically anisotropic system and that the diffraction efficiency also depends on refractive index which in this case would be accessed by the two linear modes that make up circularly polarised light.^[38]

The diffraction efficiency of the $n_{||}$ μ LCE under strain was also investigated and shown in Figure 6c. The application of strain increases the pitch and an increase in diffraction efficiency is observed due to the shift of λ_p toward 404 nm. The change in pitch is linear with respect to the applied strain. Fitting the efficiency with a linear fit, a cross-over in behavior is observed at strains close to 100%, where a change in gradient is observed (gradient = 0.67 for strains below 100% and 1.79 for strains above 100%). The change in gradient may be associated with the auxetic response in these materials causing an increase in feature height upon strain and thus an increase in $\Delta\phi$ and n_1 . Any possible effect of auxeticity is hard to deconvolute from changes in measured efficiency due to strain induced changes in λ_p , however it is interesting to note that the change in gradient occurs near the onset of the auxetic response.

2.6. Durability Testing

In Sections 2.5 and 2.6 the μ LCEs are subjected to temperatures of 240 °C and strains of 157%. The upper limit of stability of the samples was investigated via Thermogravimetric analysis by performing a temperature ramp at a rate of 10 °C min⁻¹. The onset of thermal decomposition of the samples were found to be 382 °C (Figure S2, Supporting Information). The effect of high temperature and high strains on the surface topography of the grating was assessed via AFM. Figure 7 shows AFM profile scans of the μ LCEs pre- (cyan) and post- (red) test conditions. Figure 7a,b shows the grating periodicity of a $n_{||}$ (Figure 7a) and n_{\perp} (Figure 7b) sample that has been heated to 240 °C and allowed to cool back to room temperature. The post-heating pitch and amplitude were 702 ± 10 and 53 ± 2 nm for the $n_{||}$ μ LCE which is in agreement with the pre-heating pitch and amplitude of the sample (707 ± 10 and 53 ± 3 nm). The post-heating 1st order diffraction efficiency of the device (i.e., subjected to 240 °C and taken back to room temperature) was $1.97 \pm 0.2\%$ which is agreement with the pre-heating diffraction efficiency ($1.95 \pm 0.2\%$) and

theoretical predictions for the pristine sample (1.97%). The post-heating pitch and amplitude were 989 ± 10 and 61 ± 2 nm for the n_{\perp} μ LCE meaning a reduction in both pitch and amplitude has been found when compared to the original sample (1010 ± 5 and 68 ± 3 nm). The post-heating 1st order diffraction efficiency of the device (i.e., subjected to 240 °C and taken back to room temperature) was $2.5 \pm 0.2\%$ which is lower than the pre-heating diffraction efficiency ($3.76 \pm 0.2\%$). Therefore, subjection to temperatures of 240 °C may lead to damage to the μ LCE samples. Figure 7c shows the AFM profile scan of the $n_{||}$ pre- (cyan) and post- (red) straining to 156%. The pitch and amplitude of the post-strain (i.e., strained to 156%, strain then removed and allowed to relax back to unstrained state) was 696 ± 10 nm and 50 ± 2 which is in agreement with the pre-strain values (707 ± 10 and 53 ± 3 nm).

We assessed the dimensional stability of the μ LCE gratings under repeated thermal and mechanical actuation by measuring the pitch of the $n_{||}$ μ LCE over 50 cycles. The post-cycled SRG pitch (d) compared with the original pitch ($d_0 = 707 \pm 10$ nm) of the $n_{||}$ μ LCE, measured directly after fabrication and prior to any actuation. After 50 cycles between 20 and 100 °C the thermally actuated μ LCE was found to have a pitch of 711 ± 15 nm (<1% change), relative to the original pre-cycled μ LCE dimensions. Similarly, after 50 cycles between 0% and 30%, the mechanically actuated μ LCE had a pitch of 713 ± 17 nm (<1% change).

3. Conclusion

We report tunable LCEs with sub-micron features achieved via intrinsic anisotropic deswelling. These μ LCEs were well suited as optical diffraction gratings with a high sensitivity to external thermal and mechanical stimuli. By utilizing the intrinsic anisotropic deswelling of these LCEs, a pitch anisotropy of 303 nm (1010 vs 707 nm) in a chemically identical sample was found. A pitch tunability range of 130 nm was found by altering the amount of the non-polymerizable mesogenic component of the LCE during synthesis; the lower and upper bounds being limited by the nematic-to-isotropic transition temperature, and phase separation and crystallization respectively. With further investigation this range could likely be extended by introducing other non-polymerizable mesogenic components/mixtures that suppress crystallization but have a wide temperature range in the nematic phase.

The sensitivity of the μ LCEs to thermal stimuli was investigated showing a -322 and $+212$ nm change in initial pitch for the \hat{n}_\perp and \hat{n}_\parallel respectively over a 215 °C temperature range. The sensitivity of the μ LCEs to mechanical stimuli was investigated for \hat{n}_\parallel μ LCE, showing a 167% (1110 nm) increase in pitch over its operational strain range. Diffraction efficiency measurements reveal an increase in 1st order diffraction efficiency for the n_\parallel μ LCE and a decrease in 1st order diffraction efficiency for the n_\perp μ LCE. This change is related to a change in the peak efficiency wavelength due to temperature driven changes in pitch.

The auxetic response, a known behavior in these systems, is also observed in the μ LCE gratings as confirmed by AFM, where a growth in grating height of +26%, relative to the initial height, is observed at a strain of 146%. An increase in diffraction efficiency is observed with applied strain related to the change in the peak efficiency wavelength due to strain-driven changes in pitch. A cross-over in diffraction efficiency behavior is observed at a strain of 100% which may be associated with the auxetic response increasing the depth of the surface features. For deformable diffraction gratings, a reduction in peak diffraction efficiency is observed due to a reduction in surface feature height^[12,39] Thus, the observed auxetic response in the all-acrylate μ LCEs may provide a fundamental benefit to their use as mechano-optical diffractive devices. Additionally, we expect this response will provide additional functionality to strain-tunable micro-textures in general, for example, controlling surface hydrophobicity.^[40]

Preliminary durability tests confirm the fidelity of the grating profile to thermal and mechanical stimuli up to 50 cycles. Evidence of a reduction in surface feature height is present in samples taken to 240 °C which may guide the operational range of the μ LCE for device applications.

4. Experimental Section

Fabrication of Imprinted Polyimide Grating Molds: A film-backed, linear SRG serves as the master structure for fabricating the μ LCEs in this work; the methodology is outlined in Figure 1a. The SRG film was embossed at a pressure of 3.5 MPa in to a UV-curable resin (MINS-311RM, Minuta Technology Co.) on a glass backing substrate.^[41,42] Polydimethylsiloxane (Sylgard-184, Dow Corning Inc.) with a 10:1 prepolymer-crosslinker ratio was cast and cured upon the embossed SRG, forming a soft working stamp for fabricating imprinted polyimide (IPI) LC alignment layers. A planar polyimide, SE-130 (Nissan Chemical), was spin coated at 2000 rpm for 45 s, imprinted at 75 °C for 2 mins and baked at 200 °C for 30 min. Mechanical rubbing with a cotton rubbing cloth, defines the axes of preferential director orientation on the IPI alignment layers (RD_{PI}) and the PVA (Polyvinyl alcohol, MW = 13000, Sigma Aldrich) coated Melinex 401 (DuPont Teijin) films (RD_{PVA}). Cells are assembled as shown in Figure 1b. To ensure that samples were chemically identical to compare the effect of grating orientation, a cell was constructed with a IPI surface patterned with two mutually-orthogonal SRG regions, which are homogeneously rubbed to define a global, uniform director orientation across the whole surface shown in Figure S3 (Supporting Information). Confirmation of the rubbed surface alignment dominating^[26] over any potential grating alignment of the IPI SRG,^[43] is also shown in Figure S3 (Supporting Information).

μ LCE Synthesis: Using these micro-imprinted cells, the LCEs are synthesized using the method described previously.^[29,30] The constituent chemicals of the LCEs are shown in Figure 1c, the mol.% of the chemicals were shown in Table 1. 6-(4-cyano-biphenyl-4'-yloxy)hexyl acrylate (A6OCB) was a monofunctional reactive mesogenic, 1,4-bis-[4-(6-acryloyloxyhexyloxy)benzoyloxy]-2-methylbenzene (RM82) was a mesogenic crosslinker, 2-ethylhexyl acrylate (EHA) was a monofunctional plas-

Table 1. Chemical composition of the LCE used throughout.

| Chemical name | Monomer mixture [mol.%] | Final LCE film (post wash) [mol.%] |
|---------------|-------------------------|------------------------------------|
| RM82 | 3.5 | 8.0 |
| A6OCB | 24.4 | 55.6 |
| 6OCB | 54.6 | – |
| EHA | 16.0 | 36.4 |
| MBF | 1.5 | – |

ticizer, methyl benzoylformate (MBF) was a UV-photoinitiator, and 4'-hexyloxy-4-cyanobiphenyl (6OCB) was a nonreactive mesogen that was added to broaden the nematic phase of the precursor mixture and produces a swollen LCE network. The 100 μ m thick cavity was capillary filled with the LCE precursor mixture and left to align for 20 min. The filled cell was irradiated with 370 nm UV light at 15 mW cm⁻² for 2 h to ensure complete polymerization. To form LCEs in the nematic phase, the UV polymerization step was performed at room temperature. A chemically identical isotropic LCE was synthesized using the composition in Table 1 whilst performing the polymerization step at 60 °C, which was above the nematic-to-isotropic transition of the monomer mixture (37.1 °C via DSC on cooling at a rate of 10 °C min⁻¹, Figure S4, Supporting Information), as described previously.^[20,44] After curing, the cells were opened by carefully peeling the Melinex substrate away using a scalpel. The spacers were then removed from the cell and the swollen LCEs was removed from the glass slide using flat-tipped tweezers. The swollen LCE was washed with a 70:30 methanol:dichloromethane solution. First the swollen film was submerged in a petri dish filled with methanol. Dichloromethane is slowly added step-wise until a 30% concentration was reached. The LCE was left in the methanol:dichloromethane solution for 24 h to remove the 6OCB. After 24 h the LCE films were removed from the solution and dried for 4 h at 40 °C in a fume hood to remove the excess methanol:dichloromethane solution.^[20,44]

In Section 2.2 μ LCEs with varying concentrations of 6OCB were synthesized, these are outlined in Table 2.

AFM Measurements: The surface topography of the IPI grating molds and the μ LCE films was characterized using atomic force microscopy (AFM), with a Veeco Dimension 3100 AFM in tapping mode. AFM scans accompanying Figures 2, 3, and 5 are provided in the Supporting Information.

Differential Scanning Calorimetry: Differential scanning calorimetry (DSC) was performed using a TA Instruments Q20 DSC to determine phase transitions in the precursor mixture. 10 mg of LCE precursor mixture was pipetted into a TZero Aluminum pan and an empty pan was used as a reference. DSC cycles were performed from 100 to -20 °C at a rate of 10 °C min⁻¹.

Diffraction Measurements: A 404 nm 0.5 mW laser was shone upon the μ LCEs at normal incidence with a spot size of 1.5 mm. The diffraction patterns were projected on to a screen with a millimeter scale (experimental set-up shown in Figure S8, Supporting Information). Direct measurement of the distance (x), between zeroth ($m = 0$) and first ($m = \pm 1$) order

Table 2. Pre-wash chemical composition of the LCE used in Section 2.2. The LCE marked with an asterisk is the composition used in the majority of the report.

| Chemical name | LCE-1 [mol.%] | LCE-2(*) [mol.%] | LCE-3 [mol.%] | LCE-4 [mol.%] |
|---------------|---------------|------------------|---------------|---------------|
| RM82 | 4.2 | 3.5 | 2.8 | 2.3 |
| A6OCB | 29.2 | 24.4 | 19.2 | 15.8 |
| 6OCB | 45.7 | 54.6 | 64.4 | 70.7 |
| EHA | 19.1 | 16.0 | 12.5 | 10.3 |
| MBF | 1.8 | 1.5 | 1.1 | 0.9 |

diffraction modes, along with the sample-screen separation (L), allows the diffraction angle (θ) and thus the grating pitch/period (d) to be calculated using Equation (3) and (4).^[37] This provides a means of optically tracking microscopic changes in μ LCE surface topography. Plotted in Figure 5b is the relative change in grating pitch (d) for both μ LCE varieties.

$$m\lambda = d \sin(\theta) \quad (3)$$

$$\theta = \tan^{-1}\left(\frac{x}{L}\right) \quad (4)$$

Using the diffraction setup shown in Figure S8 (Supporting Information), with the hot stage removed and the μ LCE mounted in a bespoke strain rig, the change in diffraction angle (θ) was measured as a function of applied strain. The initial length of the sample (L_0) and the strained length (L) are measured with digital callipers, from which the fractional length (L/L_0) was calculated. The grating pitch (d) was then inferred from Equation (1) using the measured values of θ .

The 1st order diffraction efficiency was calculated using a Thorlabs PM100D power meter console with a S120VC sensor. The 0th order and 1st order diffraction powers were determined and the 1st order diffraction efficiency was calculated using Equation (5).^[4,23]

$$DE_{1st} (\%) = \frac{P_{1st}}{P_{0th} + P_{1st}} * 100 \quad (5)$$

where P_{1st} is the power of the 1st order diffraction spot and P_{0th} is the power of 0th order diffraction spot. The nematic μ LCEs were birefringent materials thus, to remove the dependence of diffraction efficiency on the director orientation, circularly polarized laser light was used.

Thermogravimetric Analysis: Thermogravimetric analysis (TGA) was performed using a TA Instruments Q50 TGA to determine the decomposition temperature of the μ LCE. The μ LCE film (2 mg) was loaded into the TGA and a temperature ramp from 20 to 500 °C at a rate 10 °C min⁻¹ was performed. The degradation temperature, T_{deg} , was defined as the temperature in which 5% mass loss has occurred.

Cycle Tests: AFM and diffraction measurements were performed after thermal and mechanical cycles on the μ LCEs were performed. Thermal cycles of 20 to 100 °C at 10 °C min⁻¹ were performed on a TA Q20 DSC and the mechanical cycles were performed using a TA DMA 850 cycling between 0% and 30% strain at a rate of 3% min⁻¹.

Supporting Information

Supporting Information is available from the Wiley Online Library or from the author.

Acknowledgements

The authors would like to thank the Engineering and Physical Sciences Research Council of Great Britain for funding under research grants EP/V054724/1 and EP/T517860/1. The authors would like to thank Dr. Devesh Mistry and Prof. Helen F. Gleeson of the University of Leeds for useful discussions and guidance during this project.

Conflict of Interest

The authors declare that patent number WO2019/077361 A1 is within the scope of this work. Additionally, T. Raistrick is a shareholder in Auxetec Ltd (Company number 12925662).

Data Availability Statement

The data that support the findings of this study are openly available in <https://doi.org/10.5518/1507>, reference number [45].

Keywords

anisotropic deswelling, diffractive optical elements, liquid crystal elastomers, sub-micron features

Received: March 30, 2024

Revised: May 29, 2024

Published online: June 27, 2024

- [1] J. Wei, M. Zhu, T. Du, J. Li, P. Dai, C. Liu, J. Duan, S. Liu, X. Zhou, S. Zhang, L. Guo, H. Wang, Y. Ma, W. Huang, Q. Zhao, *Nat. Commun.* **2023**, *14*, 4839.
- [2] J. Feng, Y. Zheng, Q. Jiang, M. K. Włodarczyk-Biegun, S. Pearson, A. del Campo, *Adv. Mater. Technol.* **2022**, *7*, 2101539.
- [3] H. Zhong, Q. Xue, J. Li, Y. He, Y. Xie, C. Yang, *Adv. Mater. Technol.* **2023**, *8*, 2200947.
- [4] A. Ryabchun, M. Wegener, Y. Gritsai, O. Sakhno, *Adv. Opt. Mater.* **2016**, *4*, 169.
- [5] I. Zubritskaya, R. Cichler, I. Faniaye, D. Martella, S. Nocentini, P. Rudquist, D. S. Wiersma, M. L. Brongersma, *Adv. Mater.* **2023**, *35*, 2209152.
- [6] A. Kocabas, F. Ay, A. Dâna, I. Kiyat, A. Aydinli, *Opt. Lett.* **2005**, *30*, 3150.
- [7] A. Kocabas, F. Ay, A. Dâna, A. Aydinli, *J. Opt. A-Pure Appl. Op.* **2006**, *8*, 85.
- [8] R. M. De Oliveira Hansen, Y. Liu, M. Madsen, H. G. Rubahn, *Nanotechnology* **2013**, *24*, 145301.
- [9] M. Song, L. Feng, P. Huo, M. Liu, C. Huang, F. Yan, Y. Q. Lu, T. Xu, *Nat. Nanotechnol.* **2023**, *18*, 71.
- [10] T. Khudiyev, C. Hou, A. M. Stolyarov, Y. Fink, *Adv. Mater.* **2017**, *29*, 1605868.
- [11] Y. Wang, L. Shang, G. Chen, L. Sun, X. Zhang, Y. Zhao, *Sci. Adv.* **2020**, *6*, eaax8258.
- [12] B. Ryba, E. Förster, R. Brunner, *Appl. Opt.* **2014**, *53*, 1381.
- [13] Y. Xia, G. M. Whitesides, *Angew. Chem., Int. Ed.* **1998**, *37*, 550.
- [14] A. Guglielmelli, S. H. Nemat, A. E. Vasdekis, L. De Sio, *J. Phys. D Appl. Phys.* **2019**, *52*, 053001.
- [15] S. Sayed, P. R. Selvaganapathy, *Nanoscale Adv.* **2020**, *2*, 5461.
- [16] M. H. Lee, M. D. Huntington, W. Zhou, J. C. Yang, T. W. Odom, *Nano Lett.* **2011**, *11*, 311.
- [17] S. T. Kim, H. Finkelmann, *Macromol. Rapid Commun.* **2001**, *22*, 429.
- [18] R. Kizhakidathazhath, Y. Geng, V. S. R. Jampani, C. Charni, A. Sharma, J. P. F. Lagerwall, *Adv. Funct. Mater.* **2020**, *30*, 1909537.
- [19] Y. Huang, Y. Xu, H. K. Bisoyi, Z. Liu, J. Wang, Y. Tao, T. Yang, S. Huang, H. Yang, Q. Li, *Adv. Mater.* **2023**, *35*, 2304378.
- [20] D. Mistry, M. Nikkhou, T. Raistrick, M. Hussain, E. I. L. Jull, D. L. Baker, H. F. Gleeson, *Macromolecules* **2020**, *53*, 3709.
- [21] M. T. Brannum, A. M. Steele, M. C. Venetos, L. S. T. J. Korley, G. E. Wnek, T. J. White, *Adv. Opt. Mater.* **2019**, *7*, 1801683.
- [22] X. Zhuang, W. Zhang, K. Wang, Y. Gu, Y. An, X. Zhang, J. Gu, D. Luo, J. Han, W. Zhang, *Light Sci. Appl.* **2023**, *12*, 14.
- [23] M. Devetak, B. Zupančič, A. Lebar, P. Urnek, B. Zalar, V. Domenici, G. Ambrošič, M. Žigon, M. Čopič, I. Drevenšek-Olenik, *Phys. Rev. E Stat. Nonlin. Soft Matter. Phys.* **2009**, *80*, 050701.
- [24] B. Tašič, W. Li, A. Sánchez-Ferrer, M. Čopič, I. Drevenšek-Olenik, *Macromol. Chem. Phys.* **2013**, *214*, 2744.
- [25] P. Zhang, M. G. Debije, L. T. de Haan, A. P. H. J. Schenning, *Small* **2023**, *19*, 2302051.
- [26] Y. Choi, H. Yokoyama, J. S. Gwag, *Opt. Express* **2013**, *21*, 12135.
- [27] D. Mistry, P. B. Morgan, J. H. Clamp, H. F. Gleeson, *Soft Matter* **2018**, *14*, 1301.

- [28] T. Raistrick, Z. Zhang, D. Mistry, J. Mattsson, H. F. Gleeson, *Phys. Rev. Res.* **2021**, 3, 023191.
- [29] Z. Wang, T. Raistrick, A. Street, M. Reynolds, Y. Liu, H. F. Gleeson, *Materials* **2023**, 16, 393.
- [30] D. Mistry, S. D. Connell, S. L. Mickthwaite, P. B. Morgan, J. H. Clamp, H. F. Gleeson, *Nat. Commun.* **2018**, 9, 5095.
- [31] I. Kundler, H. Finkelmann, *Macromol. Rapid Commun.* **1995**, 16, 679.
- [32] H. Finkelmann, I. Kundler, E. M. Terentjev, M. Warner, *J. de Phys. II* **1997**, 7, 1059.
- [33] I. Kundler, H. Finkelmann, *Macromol. Chem. Phys.* **1998**, 199, 677.
- [34] E. Nishikawa, J. Yamamoto, H. Yokoyama, H. Finkelmann, *Macromol. Rapid Commun.* **2004**, 25, 611.
- [35] A. Y. Meshalkin, V. V. Podlipnov, A. V. Ustinov, E. A. Achimova, *J. Phys.: Conf. Ser.* **2019**, 1368, 022047.
- [36] E. J. Cooper, M. Reynolds, T. Raistrick, S. R. Berrow, E. I. L. Jull, V. Reshetnyak, D. Mistry, H. F. Gleeson, *Macromolecules* **2024**, 57, 2030.
- [37] C. Palmer, *Diffraction Grating Handbook*, 8th Ed., MKS Instruments, New York **2020**.
- [38] V. V. Belyaev, A. S. Solomatin, H. Margaryan, N. Hakobyan, S. Kumar, D. N. Chaousov, A. A. Belyaev, A. G. Smirnov, A. A. Gorbunov, *Applied Optics* **2020**, 59, 8443.
- [39] Y. J. Quan, Y. G. Kim, M. S. Kim, S. H. Min, S. H. Ahn, *ACS Nano* **2020**, 14, 5392.
- [40] M. Coux, C. Clanet, D. Quéré, *Appl. Phys. Lett.* **2017**, 110.
- [41] R. M. Amos, G. P. Bryan-Brown, E. L. Wood, J. C. Jones, P. T. Worthing, *Embossing Method and Apparatus*, US 7824516 **2005**.
- [42] J. C. Jones, *J. Soc. Inf. Disp.* **2008**, 16, 143.
- [43] D. W. Berreman, *Phys. Rev. Lett.* **1972**, 28, 1683.
- [44] T. Raistrick, M. Reynolds, H. F. Gleeson, J. Mattsson, *Molecules* **2021**, 26, 7313.
- [45] T. Moorhouse, T. Raistrick, Dataset associated with 'Sub-micron Diffractive Optical Elements Facilitated by Intrinsic Deswelling of Auxetic Liquid Crystal Elastomers', <https://doi.org/10.5518/1507>.